NATIONAL AERONAUTICS AND SPACE ADMINISTRATION

PROPOSED JOURNAL ARTICLE

AN ANALYTICAL AND EXPERIMENTAL INVESTIGATION OF NONADIABATIC PARTICLE LOSSES IN AXISYMMETRIC AND MULTIPOLAR MAGNETIC FIELDS

by J. Reece Roth

Lewis Research Center

National Aeronautics and Space Administration

Cleveland, Ohio

N66 29376

Prepared for

Physics of Fluids

September 13, 1965

65-56

AN ANALYTICAL AND EXPERIMENTAL INVESTIGATION OF

NONADIABATIC PARTICLE LOSSES IN AXISYMMETRIC

AND MULTIPOLAR MAGNETIC FIELDS

by J. Reece Roth

Lewis Research Center
National Aeronautics and Space Administration
Cleveland, Ohio

29376

ABSTRACT

This paper contains an investigation of the nonadiabatic behavior of a single nonrelativistic charged particle in two magnetic field geometries; an axisymmetric magnetic mirror, which was investigated by both analytical and experimental means, and a minimum-B configuration formed by the superposition of a multipolar (Ioffe) magnetic field on an axisymmetric magnetic mirror, which was studied only by analytical means. The nonlinear equations of motion for a charged particle in these magnetic field configurations were solved for 10^5 sets of initial conditions on a high-speed computer. A particle was considered to be nonadiabatic if its "adiabatic invariant" $M_4 \sim v_\perp^2/B$ varied by more than 5 percent during a single interaction with the magnetic mirror in question. By defining suitable dimensionless similarity parameters, it was found possible to summarize the computer results in a single analytical expression, which predicts the conditions under which nonadiabatic behavior will be observed as a function of the particle initial conditions. This similarity relation is a useful substitute for a closed-form solution to the nonlinear and nonholonomic mathematical problem and may be used as a basis for correlating experimental data.

An experimental technique was devised to detect the enhanced particle losses resulting from nonadiabatic particle motion in an axisymmetric magnetic mirror. The results from a wide range of experimental conditions were plotted in terms of the similarity parameters that were useful in correlating the analytical results and were found to obey the same similarity relation. This experimentally determined similarity relation gives the conditions for the onset of nonadiabatic losses in terms of the mirror ratio, particle energy, distance between mirrors, etc. This relation may be used as a design criterion to assure adiabatic confinement in all axisymmetric magnetic mirrors of practical interest.

INTRODUCTION

One of the most promising methods of confining charged particles in a localized region of space is by trapping them between two "magnetic mirrors" - regions of increasing magnetic field strength. Particles that are confined in this general class of configurations are subject to several loss mechanisms, one of which results from the nonadiabatic interaction of a single charged particle with a magnetic mirror. This paper has been motivated by the belief that nonadiabatic losses should be understood well enough to be avoided, before one can usefully proceed to study collective loss processes.

It is helpful to distinguish three types of individual particle losses from magnetic mirrors, which are illustrated by the schematic diagram of velocity space in Fig. 1: (1) adiabatic losses, which occur when the velocity vector falls within the escape cone in velocity space given by[1]

$$\theta_1 \equiv SIN^{-1} \sqrt{R_m} , \tag{1}$$

where $R_m \equiv B_{min}/B_{max}$, on the magnetic field axis, (2) nonadiabatic losses which occur after a single interaction with a magnetic mirror, and result from an increase in the size of the loss cone above its adiabatic value; such particles would have velocity vectors in the upper right of Fig. 1, and (3) nonadiabatic losses resulting from a random-walk multiple-reflection diffusion of the particle velocity vector from the confined region in the upper left of figure 1 across the boundary OABC into the loss region. Such losses would be a result of nonadiabatic effects and not of collisions. In this paper, only losses of the second type are investigated.

The method of similarity analysis has been applied to the problem of determining under what conditions single interaction nonadiabatic losses will occur from the magnetic mirror configurations that were studied. As understood in this paper, similarity analysis consists of defining nondimensional variables that characterize the physical system under study and then relating these similarity parameters to form analytical expressions, or "similarity relations", which describe the behavior of the system. This method has been successful in describing diverse phenomena in the fields of aerodynamics and heat transfer, for example, where the phenomena of interest are either too complex to be amenable to rigorous mathematical treatment, or are described by nonlinear equations that do not admit of a rigorous and general solution.

ANALYTICAL PROGRAM

Previous Investigations

The equations of motion for a charged particle in a magnetic mirror are nonlinear, and, if the "adiabatic invariant" [2,3]

$$M_4 \equiv \frac{m^2 |\mathbf{v} \times \mathbf{B}|^2}{e |\mathbf{B}|^3} = \frac{m^2 v_\perp^2}{eB} \qquad (2)$$

is constrained to vary by less than a specified amount, these nonlinear equations of motion are subject to a nonholonomic (inequality) constraint. The general mathematical problem has been studied by many investigators, nearly all of whom linearize the equations of motion by assuming that ϵ, the ratio of the raduis of gyration of the particle to the characteristic length of the magnetic field, is much less than unity. A discussion of this approach is given by Northrop[4] and by many of the references cited therein. The result of these investigations is that, if ϵ is small in the preceding sense, the adiabatic invariant M_4 is a constant of the motion, and the particle reflection conditions are then predictable in a manner originally outlined by Fermi[5] and Alfven[6]. It will be shown subsequently that ϵ is a similarity parameter of the problem if

$$\epsilon \equiv \frac{\langle R_L \rangle}{Z_o} = \frac{mv}{eB_{av}Z_o} = \frac{1}{B_{av}Z_o} \sqrt{\frac{2mV}{e}} \quad , \qquad (3)$$

Where V is the total particle energy in electron volts, $B_{av} \equiv \frac{1}{2}(B_{min} + B_{max})$, the average magnetic field on the axis, and Z_o is the axial distance between B_{min} and B_{max}.

A few investigators have relaxed the requirement that ϵ be small, and have attempted to predict the magnitude of the variation in M_4 for various magnetic fields. One such investigation was that of Grad and van Norton,[7] who have derived an expression for ΔM_4 in an idealized cusp geometry. Their results depend on the geometry of the magnetic field assumed as a starting point and do not appear to relevant to the magnetic

bottle configurations of interest in the present study.

Yoshikawa[8] derived an expression for ΔM_4 as a function of ϵ by a perturbation procedure and was able to show that, in a magnetic mirror, ΔM_4 is proportional to ϵ^2 for small values of ϵ. Unfortunately, his results are not suitable for comparison with the present work, in which a single value of ΔM_4 was chosen as a basis for computation.

In addition to the work of Yoshikawa, computer studies of the exact nonlinear problem have been reported by Garren, et al.[9] and by the present author[2,3]. The study by Garren et al. covered approximately 100 sets of initial conditions and produced the important result that the escape cone for one or a few reflections of the particle is larger than that predicted in Eq. (1) by the adiabatic theory. Not enough sets of initial conditions were considered in the Garren, et al. study to draw conclusions about the systematic trends of all the variables of interest in the problem. The previous computer study by the present author[2,3] covered 5×10^4 sets of initial conditions for a wide range of conditions in an axisymmetric magnetic mirror field. The results of this study had to be summarized in graphical form, but did give information about the systematic trends of the phenomena of interest.

Analytical Formulation of Problem

The basic axisymmetric magnetic field assumed in the numerical computations is that used previously in references 2, 3, and 9, whose vector potential is given by

$$A_\theta = \frac{B_{av}z_0}{\pi}\left[\frac{\alpha}{2} + D_1 I_1(\alpha)\cos \eta\right] , \tag{4}$$

where α and η are the dimensionless radial and axial coordinates, $\alpha \equiv \pi r/Z_o$, $\eta \equiv \pi Z/Z_o$, I_1 is the Bessel function of imaginary argument, and

$$D_1 \equiv \frac{R_m - 1}{R_m + 1} .\tag{5}$$

Equation 4 gives an infinite series of magnetic bottles that are generated by a current flowing azimuthally in a cylindrical sheet at radius $r = Z_o$ and that is sinusoidally modulated in the z-direction. These magnetic bottles are a good approximation to those in laboratory apparatus if $\alpha \lesssim 1.0$.

The multipolar magnetic field that was added to the preceding axisymmetric field is generated by n pairs of infinitely long currents located on a thin cylindrical current sheet of radius r_o. This current is assumed to be spread out in azimuthal angle and to flow in the η-direction. The vector potential of the multipolar field is then equal to

$$A_z = \frac{B_m r_o}{n} \left(\frac{\alpha}{\alpha_o}\right)^n \sin n\theta ,\tag{6}$$

where B_m is the magnetic field intensity at the multipolar current sheet due to the multipolar field alone, and α_o is the nondimensional radius of the multipolar current sheet at $r = r_o$.

If the time is nondimensionalized with respect to ω_{av}, the frequency of gyration based on B_{av}, the dimensionless time is given by

$$\tau \equiv \omega_{av} t = \frac{eB_{av}t}{m} .\tag{7}$$

If the derivative with respect to the nondimensional time τ is denoted

by $'$, i.e., $d\alpha/d\tau \equiv \overset{\prime}{\alpha}$, the Lagrangian may be written

$$L = \frac{1}{2} m(\dot{r}^2 + r^2\dot{\theta} + \dot{Z}^2) + e(\underline{A} \cdot \underline{v}) = \frac{e^2 B_{av}^2 Z_o^2}{m\pi^2} \left\{ \frac{1}{2} \left[\overset{\prime}{\alpha}^2 + \alpha^2\overset{\cdot}{\theta}^2 + \overset{\prime}{\eta}^2 + \alpha^2\overset{\prime}{\theta} \right] \right.$$

$$\left. + D_1\alpha\dot{\theta}I_1(\alpha)\cos\eta + \frac{D_2}{n}\alpha^n\overset{\prime}{\eta}\sin n\theta \right\} , \tag{8}$$

where

$$D_2 \equiv \frac{B_m}{B_{av}\alpha_o^{n-1}} = \frac{2R_m}{\pi^{n-1}(R_m + 1)}\delta \tag{9}$$

and δ is related to the radial mirror ratio

$$\delta \equiv \frac{B_m}{B_{min}}\left(\frac{Z_o}{r_o}\right)^{n-1} . \tag{10}$$

The dimensionless equations of motion are then

$$\overset{\prime\prime}{\alpha} - \alpha\overset{\prime}{\theta}^2 - \alpha\overset{\prime}{\theta} - D_1\alpha\dot{\theta}I_o(\alpha)\cos\eta - D_2\overset{\prime}{\eta}\alpha^{n-1}\sin n\theta = 0, \tag{11}$$

$$\alpha\overset{\prime\prime}{\theta} + 2\overset{\prime}{\theta}\overset{\prime}{\alpha} + \overset{\prime}{\alpha} - D_1\overset{\prime}{\eta}I_1(\alpha)\sin\eta + D_1\overset{\prime}{\alpha}I_o(\alpha)\cos\eta - D_2\overset{\prime}{\eta}\alpha^{n-1}\cos n\theta = 0, \tag{12}$$

and

$$\overset{\prime\prime}{\eta} + D_2\overset{\prime}{\alpha}\alpha^{n-1}\sin n\theta + D_2\overset{\prime}{\theta}\alpha^n\cos n\theta + D_1\alpha\dot{\theta}I_1(\alpha)\sin\eta = 0. \tag{13}$$

It is worth noting that the preceding equations of motion are intrinsically nonlinear. If the field-defining constants D_1 and D_2 were set equal to zero, the motion would be that of a particle moving in the uniform magnetic field of an infinite solenoid. A perturbation approach is not indicated, since it would necessarily restrict D_1 and D_2 to small values and exclude those large variations in the magnetic fields that are most effective in confining a plasma. The only feasible way of studying the nonadiabatic variations of M_4 is to solve the preceding set of equations on a computer by numerical integration,

pending the unlikely event of a nontrivial, closed-form, general solution of these equations.

Method of Computation

In the numerical computations, a particle was injected in the direction of $+\eta$ at the midplane $\eta = 0$ and its motion followed until it was reflected, until it escaped through the magnetic mirror at $\eta = \pi$, or until it became nonadiabatic. The position and velocities corresponding to each trajectory point from the computer solution were used to calculate the kinetic energy

$$T = \alpha'^2 + \alpha^2 \theta'^2 + \eta'^2 = \pi^2 \epsilon^2 \tag{14}$$

and the adiabatic invariant M_4 at each trajectory point. The constancy of the kinetic energy was used as a check on the round-off errors in the computation.

If M_4 at a given trajectory point was either higher or lower than all previous values, the previous extreme value was replaced with the new extreme value. When the ratio of the extreme values of M_4 was

$$\Delta M_4 = \left| \frac{M_{4,\ high} - M_{4,\ low}}{M_{4,\ low}} \right| \geq 0.05, \tag{15}$$

the particle was considered to be nonadiabatic, and the computation of that particular particle was terminated. The azimuthal angle θ was set equal to zero for all but a few cases, since a set of computations for various values of θ indicated that a particle was most nonadiabatic if it was injected at $\theta = 0$.

The 20 sets of velocity initial conditions listed in Table I were used for all computations. These initial conditions lie on the $+\eta$ hemisphere in velocity space, whose radius is scaled by the factor ϵ,

as indicated by Eq. (14). The dependent variable of the numerical computations was F, the fraction of the 20 "particles" that were adiabatic for given values of the initial conditions α, θ, η, ϵ, $D_1(R_m)$, $D_2(\delta)$, and n. These 20 points gave essentially the same results as the 85 used previously in references 2 and 3. Fewer than 20 initial conditions did not satisfactorily simulate an isotropic velocity distribution in velocity space.

Correlating the Results of the Numerical Computations

In the numerical computations, the initial nondimensional radius α was assigned eight values over the range $0.05 \leq \alpha \leq 2.50$; the adiabatic parameter ϵ assumed six values over the range $0.01 \leq \epsilon \leq 0.06$; the parameter R_m took on from six to twelve values over the range $0.1 \leq R_m \leq 1.00$; the parameter δ assumed six values over the range $0. \leq \delta \leq 1.50$, and the parameter n took on two values, n = 2 (quadrupole configuration), and n = 3, (hexapole configuration). This came to about 5000 cases, or, since there are 20 trajectories per case, 10^5 individual particle trajectories. A limited number of computations were made for n > 3 and $\theta \neq 0$, to assess the influence of these parameters on F, the fraction adiabatic.

Clearly, such a mass of data connot be properly interpreted without some means of correlating it, so that the relative importance of the variables and their systematic relation to one another is evident. The dimensionless variables α, ϵ, R_m, δ, n, and F are a set of similarity parameters for the problem. A sample similarity plot will be discussed to illustrate the method of correlating the data. In Fig. 2 is shown a plot of F, the fraction adiabatic, as a function of the mirror

ratio R_m, for the particular values $\delta = 0.25$, $n = 2$, $\alpha = 1.50$, and $\epsilon = 0.02$. The seven values of R_m plotted in Fig. 2 represent seven different computer runs, each of which used the 20 sets of initial conditions listed in Table I.

The value of R_m corresponding to $F = 0.10$, 0.5, and 0.9 adiabatic was read off Fig. 2 and plotted in Fig. 3, which also contains data from five other plots similar to Fig. 2, over the range $0.01 \leq \epsilon \leq 0.06$. The data for a given percentage adiabatic lie along a straight line, which implies a similarity relation of the form

$$R_m = \left(\frac{\epsilon}{\epsilon_0}\right)^A .$$
(16)

In order to improve the objectivity and precision of the curve fitting of this data, a computer program was devised that fitted a least-squares straight line to the logarithms of ϵ and R_m. Figure 3 illustrates the particular values $n = 2$, $\delta = 0.25$, and $\alpha = 1.50$. The similarity relation of Eq. (16) held for all values of n, δ, F, and α investigated. The parameters A and ϵ_0 were cross-plotted as functions of α and F, and it was found that Eq. (16) can be expressed in the form

$$R_m = \left[\frac{\epsilon}{C_1(1 - F)^{D_5} + C_2(1 - F)^{D_6}}\right]^{A_{oa}(1-F)^{D_3}} \exp\left[K_o\alpha(1-F)^{D_4}\right] ,$$
(17)

where C_1, C_2, D_5, and D_6 are functions of α, δ, and n, and are listed on Table II. The parameters A_{oa}, D_3, K_o, and D_1 are functions only of n and δ, and are listed on Table III. Equation (17), which was derived by an empirical process of curve fitting, is the desired similarity relation that, together with the values of the constants listed in Tables II and III, summarizes the behavior of the approximately 10^5

particles whose trajectories were followed by numerical computation.

Equation (17) may be thought of as a particular solution to the original nonlinear and nonholonomic mathematical problem. The procedure used here makes it possible to test how well Eq. (17) agrees with the exact solutions from which it was derived. The agreement of the exact soltuions with the value calculated from Eq. (17) was measured by the quantity

$$\Delta \equiv \frac{R_{m,e} - R_m}{R_{m,e}} \qquad (18)$$

where R_m is the value calculated by substituting the appropriate value of ϵ and the corresponding parameters from Tables II and III into Eq. (17), and $R_{m,e}$ is the mirror ratio from the exact computation, taken from the raw data charts such as Fig. 2. The number of cases in each interval of Δ is shown in Fig. 4. The distribution of error in Fig. 4 in roughly Gaussian, with a standard deviation of $\pm 6\%$. It is not possible to distinguish, in the present investigation, between errors caused by interpolating between the computer-derived data points on the raw data plots similar to Fig. 2, and errors which come about because Eq. (17) is not a general solution to the nonlinear and nonholonomic problem. It is interesting to note that most, if not all, of the 6% error could be explained by interpolation errors on the raw data plots.

The results of the numerical computation cannot be expected to correspond exactly to the results obtained in real devices for at least two reasons: (1) The definition of adiabaticity, $\Delta M_4 \leq 5\%$, is an arbitary one, and there is no a priori reason to expect this particular value of ΔM_4 to be intimately related to whether or not an ensemble of

particles are reflected or not. (2) The magnetic fields assumed in the

computations were chosen for mathematical simplicity, and, especially for

extreme values of the parameters defining them, do not correspond to actual

devices. Equation (17) is useful because it suggests the similarity

parameters that should be used in expressing the results of laboratory

experiments on nonadiabatic particle motion.

EXPERIMENTAL PROGRAM

Results from Previous Experiments

The data relating to adiabaticity from previous experiments are plotted

in Figs. 5 and 6 in terms of the similarity parameters ϵ , R_m , and α .

For later reference, the best-fit curve for the data of the present

experiment is also shown.

A study of particle confinement was reported by Gibson, Jordan, and

Lauer,[10] who trapped MEV positrons for several seconds in the magnetic

bottle formed between two current loops. They were able to measure the

decay of the positron density that resulted from the multiple-reflection

nonadiabatic diffusion of the velocity vectors into the escape region of

velocity space. It should be emphasized that even the most nonadiabatic

case shown in figures 5 and 6 for this experiment refers to particles that

were confined for several seconds on the average, so that multiple-reflection

nonadiabatic diffusion into the loss region is a relatively slow process

on the time scale of a single reflection between mirrors.

A similar experiment was reported by Rodionov,[11] who also studied the

nonadiabatic losses of positrons from a magnetic bottle configuration.

His data for adiabatic motion lie between the solid squares in Fig. 6,

and for nonadiabatic motion between the open squares in the same figure.
Unfortunately, the nature of the apparatus and the experimental technique
severely limited the accuracy with which the variables were measured.

Alexeff[12] has reported adiabatic confinement for the conditions
plotted as the solid right triangles in Figs 5 and 6. This experiment
consisted of energetic electrons trapped between magnetic mirrors.
Presumably the only loss mechanism operating in this experiment was
collisional scattering into the loss cone, although the method of
distinguishing between nonadiabatic and collisional losses was not reported.

A. C. England and his colleagues[13,14] have reported the behavior
of microwave heated electrons in the "EPA" and "PTF" mirror machines at
Oak Ridge. In both machines, there was a core of $\approx$100 KEV electrons near
the axis that appeared to be adiabatically confined, and higher energy
electrons - in the MEV energy range - near the outskirts of the plasma
that appeared to be subject to nonadiabatic losses. The energy of the
electrons that were subject to nonadiabatic losses was uncertain by about
a factor of 2. The range of values for which nonadiabatic motion was
observed is plotted as the open triangles in Fig. 6. The solid triangles
represent conditions under which adiabatic motion was observed.

The experiments reported in references 2 and 3, unlike the experiments
described in the preceding paragraphs, were designed to study a single
interaction of a particle with a magnetic mirror. The experimental technique
used in these experiments was crude, since it only attempted to measure
the conditions under which nonadiabatic losses became large compared
with the usual adiabatic losses. The experimental technique was not

sufficiently sensitive to measure the onset of nonadiabatic losses, as was

done in the experiments reported below; and this fact explains the

discrepancy with the current experiment. The data from references 2 and

3 are plotted as diamonds in Fig. 5. These diamonds mark the adiabatic-to-

nonadiabatic transition, and correspond to the point between the solid and

open symbols in the other experiments. The apparatus used in references

2 and 3 restricted the data to radii very close to the axis of the

magnetic field.

The incompleteness of the previous experimental results made it

desirable to measure systematically the ϵ appropriate to the adiabatic-

to-nonadiabatic transition as a function of the mirror ratio R_m and the

average radius at which the particle moves, α . Such a series of

experiments was undertaken, subject to the constraint that only axisymmetric

geometries could be investigated with the existing apparatus.

Experimental Apparatus

The ion source used in this experiment was a "modified Penning source",

similar to that described by Meyerand and Brown.[15] This source has the

useful property that it will provide a beam of ions of any gaseous material,

and can be reconnected to operate as an electron gun. The elements of this

ion source are shown in Fig. 7. About half the data was taken with He^{+} ions,

half with electrons, and two runs with Ne[+] ions. The ion collector consisted

of a Faraday cup with a 6.4-mm-diameter hole in the end that faced the ion

source. A grounded disk with a 6.4-mm-diameter hole was mounted on the end

of the Faraday cup. The axis of the Faraday cup was coincident with the

axis of the ion source, and this common axis could be positioned at any

desired radius parallel to the axis of the magnetic field. The background gas pressure was no higher than 5×10^{-7} torr, and the particle currents were, in all cases, below 10 μA. The charged particle densities were too low for collisions or other collective effects to influence the outcome of the experiment.

The axial profile of the magnetic field was measured with a 1 percent accuracy rotating-coil Gaussmeter, which yielded the experimental parameters R_m, B_{av}, and Z_0. A schematic drawing of the electrical connections of the ion source and collector is shown in figure 7. The collector was kept biased at +75 V dc to suppress secondary electrons. The ion source could be biased to 18 KV above ground, which provided an electric field between the ion source and collector. It can be shown that the electric field existing between the source and collector will not significantly influence the angular spread of the ion velocity distribution in velocity space. The ions had energies below 100 EV on leaving the source, and the ion current from the source was not a function of the bias voltage above a bias voltage of 700 volts. The y-axis of an X-Y recorder was connected to indicate the current flowing to the collector, while the x-axis indicated the ion source bias voltage. When the ions entered the Faraday cup, they were no longer acted on by electric fields and interacted only with the magnetic field. The radius gyration of the ions was, in all cases, less than the inner diameter of the Faraday cup, and the length of the cup was in all cases longer than Z_0.

In the present series of experiments, all variables except the ion energy were held constant during a given run. Ions were accelerated to a given energy, entered the Faraday cup, interacted with the magnetic field, and a certain fraction were reflected back out the same 6.4-mm-diameter

hole through which they entered. In the adiabatic regime of operation,
the fraction of particles reflecting back out of the Faraday cup was
independent of the ion energy and hence independent of ϵ. As the energy
increased to the point where nonadiabatic motion began, the escape cone
opened up, and fewer particles were reflected back out the hole in the
Faraday cup. The indicated ion current to the collector is therefore
constant up to a critical energy, corresponding to point A in Fig. 1,
and then increases as the escape cone opens up.

This behavior is illustrated on Fig. 8, which is one of the X-Y
recordings that form the raw data of this experiment. In the region
below about 4 KV, the collected ion current is constant, so that the escape
cone angle is not a function of energy. Above 4 KV, however, the
collected ion current is a ramp function, which indicates that the escape
cone angle was opening up as the particle energy (and hence ϵ) increased.
The energy at which the ion current is no longer a constant is the
"critical" energy, above which nonadiabatic losses occur. It should be
noted that this experimental technique gives information only about a
single interaction of a particle with the magnetic barrier in question.

<center>Experimental Results</center>

The experimentally obtained values of ϵ , which correspond to the
critical energy of point A in Fig. 1, have been plotted as a function of
R_m in Figs. 9 and 10 for two representative values of α . A representative
curve from the computer results, to be discussed later, is also shown.
Data were taken at eight different values of α . The data obey the
similarity relation of Eq. (16) and were fed into the same least-squares

curve-fitting program used to fit the analytical results. The "best fit"
values of A and ϵ_O for each of the eight radii investigated are
listed in Table IV, along with the number of experimental data points
taken at the radius in question.

The uncertainties in measuring the particle energy, B_{av} and Z_O
give rise to error limits on ϵ of no more than $\Delta\epsilon = \pm15\%$. The
errors in the radial position were such as to give $\Delta\alpha = \pm0.15$, a fixed
rather than a proportional error. The range of the principal experimental
variables was $0 \leq \alpha \leq 1.75$, $0.175 \leq R_m \leq 0.945$, $0.059 \leq Z_O \leq 0.241$ m,
$1/1837 \leq m \leq 20$ AMU, $0.029 \leq B_{av} \leq 1.89$ Wb/m^2, and $1500 \leq V \leq 7800$ eV.

The parameter A from the experimental curves is shown plotted as
a function of α in Fig. 11(a). The parameter A can be correlated by
the relation

$$A = A_O e^{P_1 \alpha} \tag{19}$$

where $A_O = 0.388$ and $P_1 = -0.167$. The parameter ϵ_O for the
experimental data is shown plotted as a function of α in Fig. 11(b).
ϵ_O can be correlated by the relation

$$\epsilon_O = \epsilon_{o1} e^{P_2 \alpha} \tag{20}$$

where $\epsilon_{o1} = 0.343$ and $P_2 = 0.075$. The anomalous point at $\alpha = 1.50$
was discarded in both correlations, since it was based on many fewer
experimental points than those for which $\alpha \leq 1.00$. The results of the
current series of experiments can be summarized in analytic form by the
statement that single interaction nonadiabatic losses will not occur in

axisymmetric geometries if

$$R_m \geq \left(\frac{\epsilon}{0.343e^{0.075\alpha}}\right)^{0.388e^{-0.167\alpha}} , \tag{21}$$

where the present experiments have mapped out the curve given by the equality sign.

The line which best fits the results of the present experiments is plotted in Figs. 5 and 6 for comparison with the findings of previous experiments. In the author's opinion, the instances of disagreement are attributable to the presence of one or more of the following factors in the previous experiments: (1) uncertainties in the determination of the relevant experimental variables, (2) inability to distinguish between nonadiabatic losses and losses due to other effects, such as collisions, for example, (3) inability to detect nonadiabatic losses until they became comparable to the adiabatic and/or collisional losses (corresponding to point "B" in Fig. 1), and (4) relativistic effects, which were present in the experiments reported in references 10, 13, and 14.

Within the limitations of the data, one may conclude that the analytical problem considered here and the preceding experimental results are both correlated by the same similarity parameters and by the similarity relation of Eq. (16). It therefore appears that the similarity relations and the similarity parameters appropriate to the problem of nonadiabatic particle losses have been established, and that the constants have been found for the special case of the axisymmetric geometry. The fact that the critical values of ϵ for electrons, He^{+} ions, and Ne[+] ions, with their greatly different masses, fall along the same similarity relation is

further evidence in support of this result.

DISCUSSION AND CONCLUSIONS

In the introduction, nonadiabatic particle losses were divided into single interaction nonadiabatic losses and multiple reflection nonadiabatic losses. Single interaction nonadiabatic losses were observed in the numerical computations of Garren, et al.[9] in the experiment reported in references 2 and 3 and in the present series of experiments. The latter employs an experimental technique that demonstrates this mode of nonadiabatic loss. Multiple-reflection nonadiabatic losses were observed in the experiments of Gibson, Jordan, and Lauer[10] and of Rodionov.[11] In both experiments the confined positrons were not lost until after approximately 10^8 reflections. The existence of these two modes of nonadiabatic particle loss may therefore by regarded as experimentally established.

It can be seen from an examination of Fig. 9 and Eq. (17) that, although the numerical and experimental results obey the same similarity relation, the numerical constants in the similarity relation are different and yield different slopes and intercepts. In the particular case $\alpha = 0$, shown in Fig. 9, the numerical and experimental curves cross in the vicinity of $R_m = 0.515$ for $F = 0.5$ adiabatic, $\delta = 0$. At this mirror ratio, at least some particles are lost when their adiabatic invariant M_4 varies by 5% during a single interaction with the magnetic mirror. In the range $0.515 \leq R_m \leq 1.0$, the experimental points lie to the right of the numerical curve, suggesting that in this region nonadiabatic losses occur only if M_4 varies by more than 5% during a single interaction

with the magnetic mirror field. In the range $0 \leq R_m \leq 0.515$, nonadiabatic

losses will occur if M_4 varies by less than 5% during a single interaction

with the magnetic mirror.

By studying the similarity relation of Eq. (17) and its associated

parameters in Tables II and III, the general trends of adiabaticity with

the various parameters may be exhibited. If all other factors are held

constant, the critical energy (above which nonadiabatic motion occurs) is

a monotonically decreasing function of δ , the radial mirror ratio. This

comes about because the multipolar contribution increases the unevenness

of the magnetic field. If all other factors are constant, the critical

energy at a given radius in the field is a monotonically increasing

function of n , the number of pairs of multipolar conductors. This arises

because the multipolar field is proportional to $(\alpha/\alpha_0)^{n-1}$. As n becomes

very large, the critical energy approaches that of an axisymmetric field,

as an upper bound. These findings imply that nonadiabatic losses will

increase if multipolar fields are added to a basic axisymmetric magnetic

field.

If all other factors are constant, a variation in R_m of a factor

of 2 will change the critical energy by a factor of about 100. If the

critical energy is changed by a factor of 2, the critical mirror ratio

will change by about 11%. The critical energy is therefore a very

strong function of the mirror ratio, which implies that the selection

of a mirror ratio for a device should be a matter for careful study.

Under typical conditions, the critical energy is practically independent

of radius out to some point where it becomes monotone decreasing, if all

Other factors are held constant.

Stability considerations play a role in determining the optimum value of ϵ . It has been shown by Kuo, et al.[16] that the stability of a plasma is enhanced if $\epsilon \geq 0.10$ (the so-called finite Larmor radius stabilization) and that this stabilizing effect is not present if $\epsilon \approx 0$, as the adiabatic theory requires. Finite radius of gyration stabilization therefore requires ϵ to be as large as possible. On the other hand, if ϵ is too large, the resulting nonadiabatic losses will enlarge the escape cone and make the velocity distribution of the confined particles more anisotropic than it would otherwise be. Harris[17] has shown that anisotropies in velocity space promote the growth of instabilities. Therefore, ϵ should be made small enough to avoid nonadiabatic losses, in order to reduce anisotropies in velocity space to a minimum. From the preceding discussion, it is evident that the above stability considerations dictate that ϵ should be as large as possible, without being so large that nonadiabatic losses occur. A consideration of economic factors leads to much the same conclusion, since an adiabatic mirror with large ϵ is less expensive than an adiabatic mirror with small ϵ .

The experimental results given in the preceding paragraphs can serve as criteria for the design of axisymmetric magnetic mirrors that will suffer no nonadiabatic particle losses and that will be a best compromise between the stability constraints. To confine the maximum number of particles that the adiabatic theory allows, the apparatus should operate under conditions such that Eq. (21) is satisfied. If the nonadiabatic losses caused by multiple-reflection diffusion of the velocity vector are to be

avoided, the data of Gibson, Jordan, and Lauer[10] in Fig. 5 indicate that the critical values of R_m given by Eq. (21) should be increased by about 8%.

The preceding experimental results were obtained in an axisymmetric magnetic field and must be applied with caution to the combined axisymmetric plus multipolar magnetic fields used in the numerical computations. Since the combined field is less adiabatic than an axisymmetric magnetic field alone, the experimental results should be regarded as an upper bound on ϵ, or a lower bound on R_m, the exceeding of which will certainly result in nonadiabatic losses from the combined geometry. The quantitative effects of δ and n on the adiabatic-to-nonadiabatic transition line remains to be investigated in a further series of experiments.

<div align="center">REFERENCES</div>

1. S. Glasstone and R. H. Lovberg, "Controlled Thermonuclear Reactions" D. Van Nostrand, Company, Inc., Princeton, N. J., 1960, p. 344.

2. J. R. Roth, Phys. Fluids 7, 536, (1964).

3. J. Reece Roth, Ph. D. Thesis, Cornell University, (1963).

4. T. G. Northrop, "The Adiabatic Motion of Charged Particles"(Interscience Publishers, Inc., New York, 1963).

5. E. Fermi, Phys. Rev. 75, 1169 (1949).

6. H. Alfvén, "Cosmical Electrodynamics" (Clarendon Press, Oxford, England, 1950).

7. H. Grad and R. Van Norton, Nucl. Fusion, Suppl. Pt. 1, 61 (1962).

8. S. Yoshikawa, Massachusetts Institute of Technology Research Laboratory of Electronics Quarterly Progress Report No. 55, 27 (1959).

9. A. Garren, R. J. Riddell, L. Smith, G. Bing, L. R. Henrich, T. G. Northrop, and J. E. Roberts, "Proceedings of the Second United Nations Conference on the Peaceful Uses of Atomic Energy" (United Nations, Geneva, Switzerland, 1958), 31, p. 65.

10. G. Gibson, W. C. Jordan, and E. J. Lauer, Phy. Fluids 6, 116 (1963).

11. S. N. Rodionov, J. Nucl. Energy, Pt. C 1, 247 (1960).

12. I. Alexeff, private communication.

13. A. C. England, private communication.

14. R. A. Dandl, A. C. England, W. B. Ard, H. O. Eason, M. C. Becker, and G. M. Haas, Nucl. Fusion 4, 344 (1964).

15. R. G. Meyerand, Jr., and S. C. Brown, Rev. Sci. Instr., 30, (1959).

16. L. G. Kuo, E. G. Murphy, N. Petravić, and D. R. Sweetman, J. Nucl. Energy, Pt. C, 6, 505 (1964).

17. E. G. Harris, J. Nucl. Energy, Pt. C, 2, 138 (1961).

TABLE I. - VELOCITY INITIAL CONDITIONS OF 20 PARTICLES

USED TO DETERMINE FRACTION OF PARTICLES ADIABATIC

[Particles lie on a hemisphere in velocity space,

the radius of which is scaled by the factor ϵ.]

$\dot{\eta}$	$\dot{\alpha}$	$\alpha\dot{\theta}$
0.	0.7071068	0.7071068
.05	.7062223	-.7062223
.10	.7035624	.7035624
.15	.6991008	-.6991008
.20	.6928203	.6928203
.25	.6846532	-.6846532
.30	.6745369	.6745369
.35	.6623821	-.6623821
.40	.6480741	.6480741
.45	.6314665	-.6314665
.50	.6123724	.6123724
.55	.5905506	-.5905506
.60	.5656854	.5656854
.65	.5373546	-.5373546
.70	.5049752	.5049752
.75	.4677072	-.4677072
.80	.4242641	.4242641
.85	.3724916	-.3724916
.90	.3082207	.3082207
.95	.2207940	-.2207940

TABLE II. - PARAMETERS FOR RELATION

$$\epsilon_o = C_1(1 - F)^{D_5} + C_2(1 - F)^{D_6}$$

n	δ	α							
		0.05	0.25	0.50	0.75	1.00	1.50	2.00	2.50
					D_5				
2	0.0	0.0258	0.5236	0.3916	--	0.2839	0.2536	0.3454	0.2038
	.25	.0903	.2012	.2170	0.3647	.4384	.5492	.4000	.3978
	.50	.5582	.5568	11.614	.5704	1.0177	.8782	1.3626	.2448
	.75	1.0335	.6847	.6195	.5220	.9346	-.05138	.1718	.4659
	1.00	1.2321	.6448	.7525	-.1363	1.8897	16.622	2.4956	.03562
3	0.25	0.02667	0.5062	0.2089	0.2235	0.3482	0.3831	0.6569	0.5988
	.50	.0734	-.3534	.0405	.2367	.5877	.9874	1.5270	.6490
	.75	.05788	.7581	.1839	.3190	.7365	.9338	-.4688	--
	1.00	.05418	-.4583	.3154	.4497	.8171	8.5420	4.3001	--
	1.50	.0759	.1116	.4267	.7690	1.1286	--	--	--
					D_6				
2	0.0	0	0	0	--	0	0	0	0
	.25	0	6.7397	5.2395	15.437	0	0	3.00	0
	.50	0	10.580	.7473	7.3325	0	0	0	6.4114
	.75	0	12.635	20.383	12.707	0	3.0339	6.5305	0
	1.00	11.593	15.015	16.356	4.3589	0	1.7011	0	0
3	0.25	0	0	4.9492	0	0	0	0	0
	.50	0	1.3711	4.2707	9.5029	0	0	0	19.241
	.75	0	0	6.4544	7.5818	0	17.078	4.2419	--
	1.00	0	2.1070	10.265	10.295	24.247	.5696	0	--
	1.50	0	2.3026	7.9846	15.012	16.474	--	--	--

TABLE II. - Concluded. PARAMETERS FOR RELATION

$$\epsilon_o = C_1(1 - F)^{D_5} + C_2(1 - F)^{D_6}$$

n	δ	α							
		0.05	0.25	0.50	0.75	1.0	1.5	2.0	2.5
					C_1				
2	0.0	0.1776	0.4268	0.2964	---	0.1765	0.1768	0.1801	0.1594
	.25	.1566	.1979	.1630	.1771	.1737	.1835	.1450	.1714
	.50	.1602	.1641	.4555	.1517	.1994	.1802	.2555	.1317
	.75	.1763	.1405	.1290	.1214	.1688	.06355	.1012	.1918
	1.00	.1581	.1033	.1200	.04584	.2260	.5855	.2627	.1738
3	0.25	0.1699	0.3967	0.2097	0.1871	0.1633	0.1597	0.1769	0.1688
	.50	.1737	.05973	.1503	.1507	.1749	.1924	.2215	.1339
	.75	.1681	.4602	.1540	.1356	.1695	.1404	.04368	--
	1.00	.1692	.05625	.1563	.1317	.1495	.2381	.3800	--
	1.50	.1662	.1225	.1358	.1341	.1455	. --	--	--
					C_2				
2	0.0	0	0	0	--	0	0	0	0
	.25	0	0.3130	0.3459	0.3935	0	0	0.100	0
	.50	0	.6289	.1757	.1614	0	0	0	0.1420
	.75	0	.9573	1.6626	.3435	0	.1408	.2123	0
	1.00	0.2268	2.3105	.8866	.2906	0	.1672	. 0	0
3	0.25	0	0	0.2250	0	0	0	0	0
	.50	0	0.3945	.3007	0.1985	0	0	0	0.7337
	.75	0	0	.2888	.2153	0	0.2660	0.2191	--
	1.00	0	.5475	.3704	.2524	.4173	.0981	0	--
	1.50	0	.3220	.4350	.4688	.4467	--	--	--

TABLE III. - CONSTANTS FOR RELATIONS

$$A_o = A_{oA} (1 - F)^{D_3} \text{ and } K = K_o (1 - F)^{D_4}$$

n	δ	A_{oA}	D_3	K_o	D_4
2	0.0	0.5895	0.0805	-0.8004	-0.0892
	.25	.6600	.0884	-.8858	-.0510
	.50	.6790	-.1000	-.9549	-.0656
	.75	.7286	-.1048	-1.0014	-.1010
	1.00	.6256	-.4501	-.8383	-.4837
3	0.25	0.5994	0.1508	-0.8116	0.0208
	.50	.6304	.0674	-.870	.020
	.75	.6369	.0515	-.8266	-.0772
	1.00	.6620	.0895	-.8991	.1205
	1.50	.6752	.0386	-.8277	-.1182

TABLE IV. - PARAMETERS ϵ_O AND A FOR BEST

FIT TO DATA FROM PRESENT EXPERIMENT

α	ϵ_O	A	Number of data points
0.0	0.3473	0.3854	49
.25	.3551	.3731	48
.50	.3580	.3670	35
.75	.3692	.3435	33
1.00	.3725	.3265	23
1.25	.4022	.2916	17
1.50	.3518	.4904	6
1.75	.4036	.3062	6
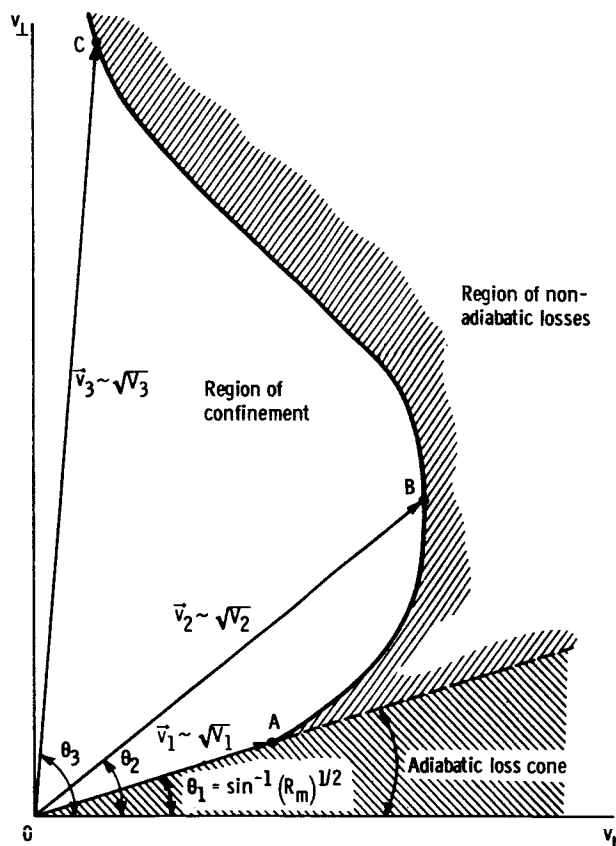
Figure 1. - Nonadiabatic loss regions in velocity space. V_1, transition energy at which nonadiabatic losses start to occur; V_2, energy at which substantial nonadiabatic losses occur; V_3, energy at which virtually all particles are lost nonadiabatically.
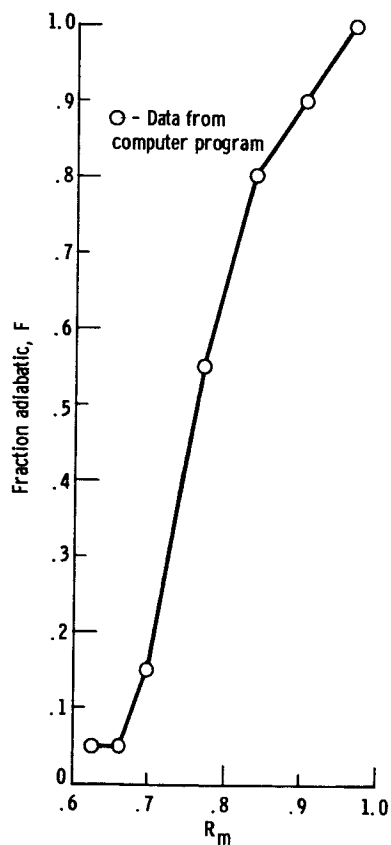
Figure 2. - Fraction of particles adiabatic as function of R_m for conditions $\delta = 0.25$, $n = 2$, $\alpha = 1.50$, and $\varepsilon = 0.02$.

	F	A	ε_0
○	0.1	0.177	0.177
□	.5	.152	.123
◇	.9	.113	.0608
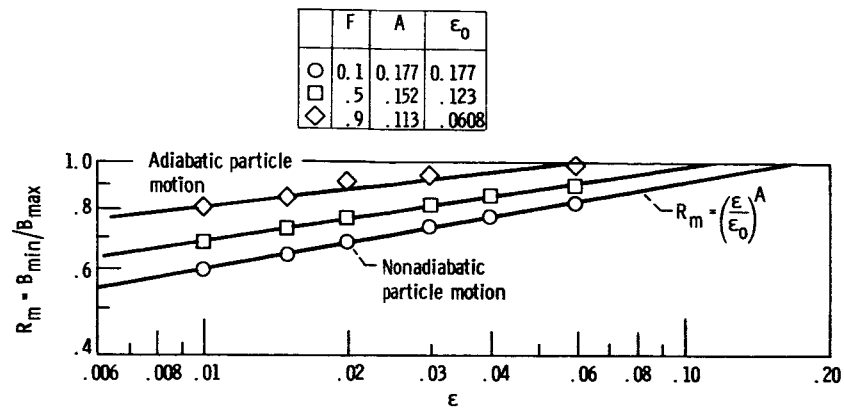
Figure 3. - Mirror ratio R_m as function of ε for $F = 0.1$, 0.5, and 0.9; $n = 2$; $\alpha = 1.50$; and $\delta = 0.25$.
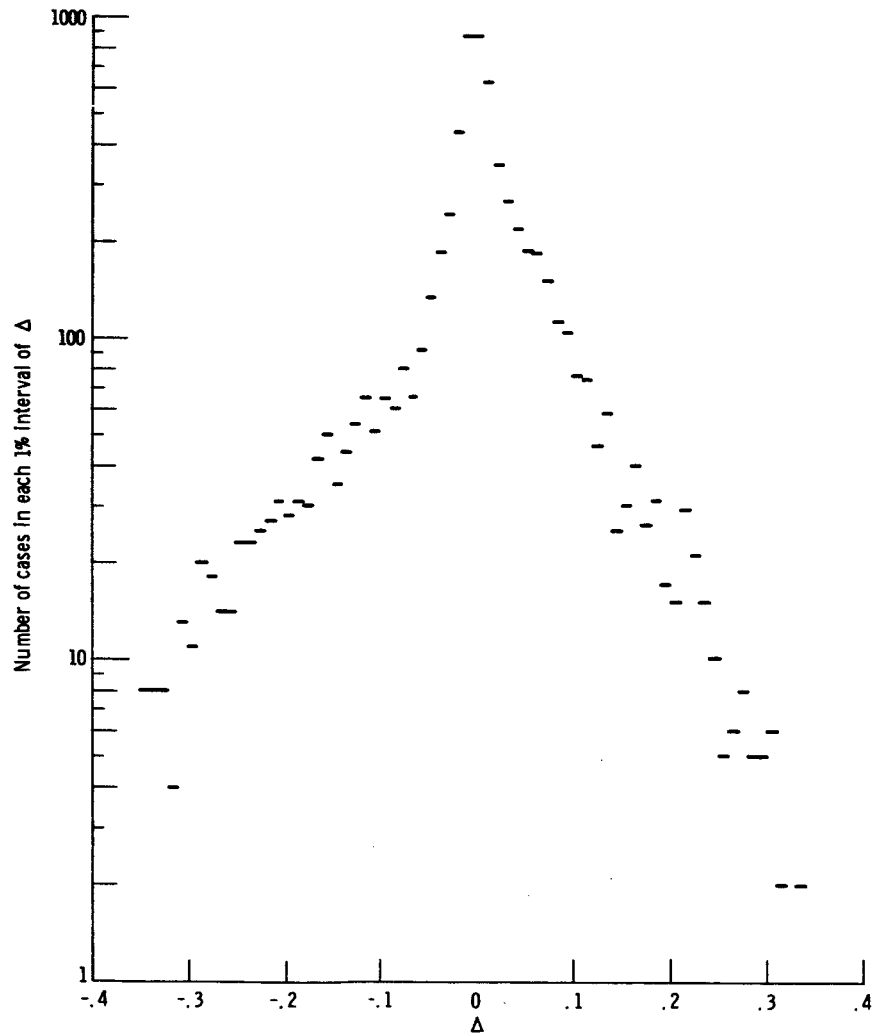
Figure 4. - Number of cases within each 1% interval of Δ showing agreement of Eq. (17) with actual calculated values. Total cases, 6548.
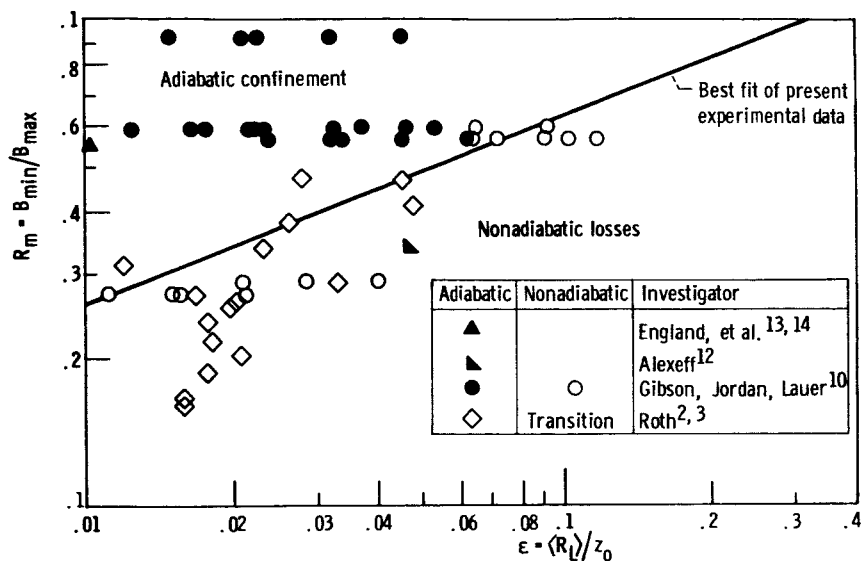
Figure 5. – Prior experimental data for $\alpha = 0$.
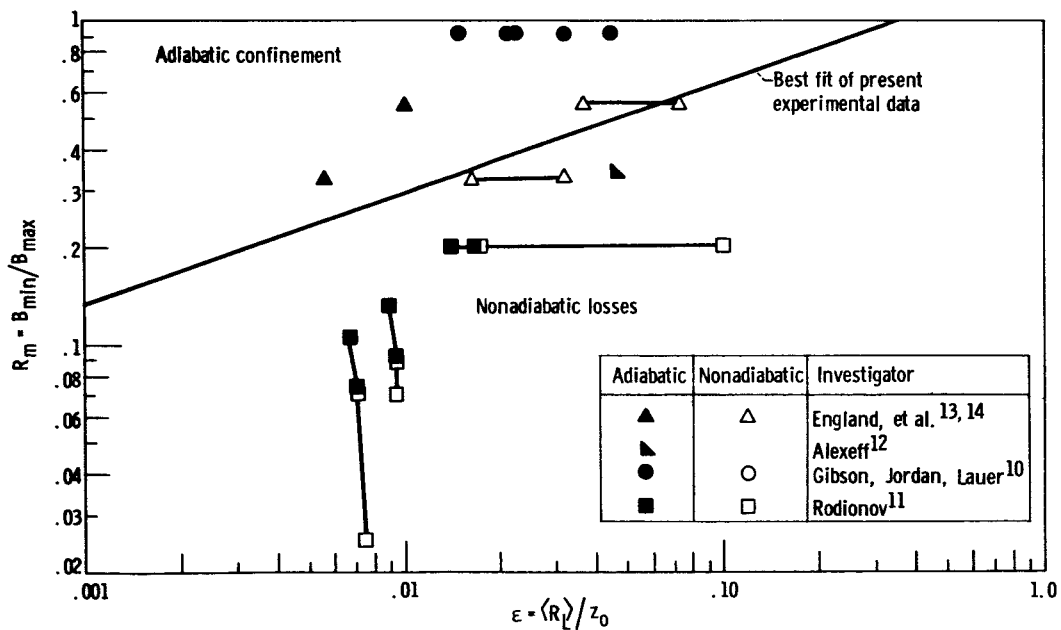
Figure 6. – Prior experimental data for $\alpha = 0.75$.

B, on axis   B = B_{min} B = B_{av} B = B_{max}

z

z_0

Magnetic field coils

Floating d-c filament supply

Ion source

$\alpha = \pi r / z_0$

r

45 V (dc)

Ion collector

₵

Floating anode supply 0 to 1 kV (dc)

75 V (dc) bias

x Input

X-Y recorder

y input

High-voltage bias supply 0 to 20 kV (dc)
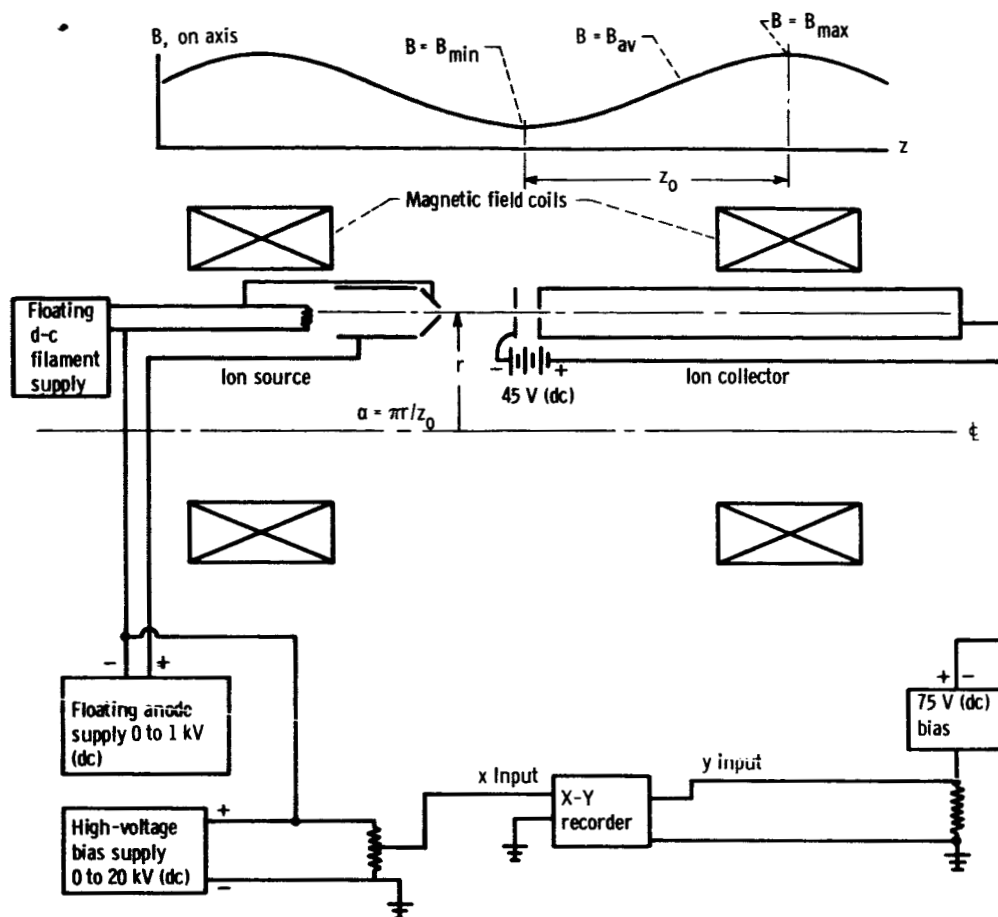
Figure 7. – Schematic diagram of experimental apparatus.

Relative collector current, arbitrary units

3.5

3.0

2.5

2.0

1.5

0   2   4   6   8 10×10^3

Ion energy, eV

Nonadiabatic losses occuring

Adiabatic reflection
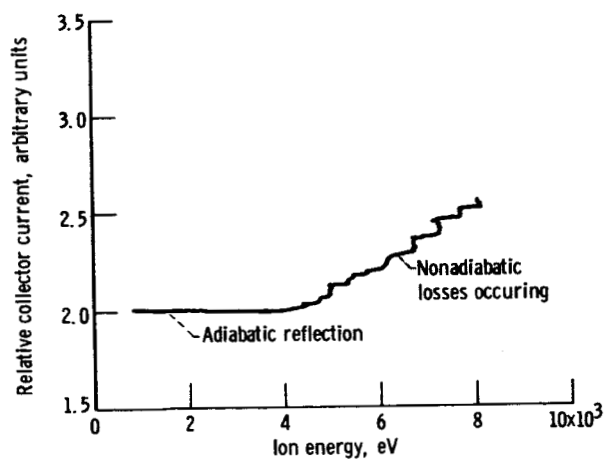
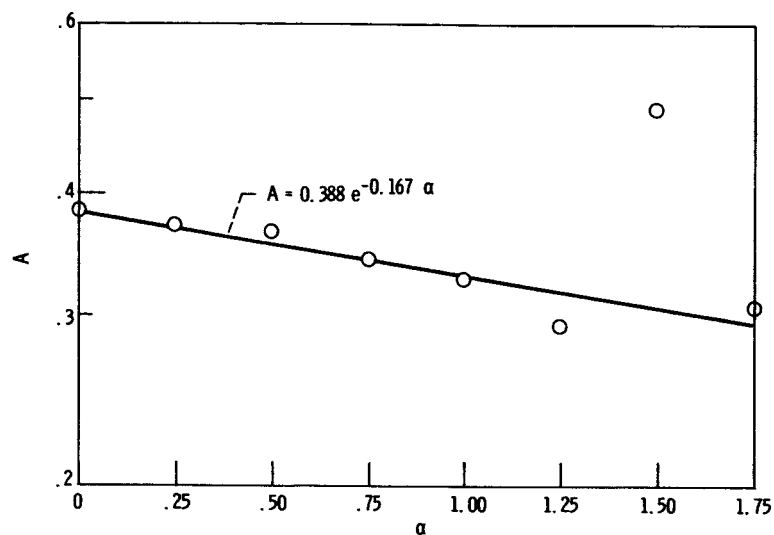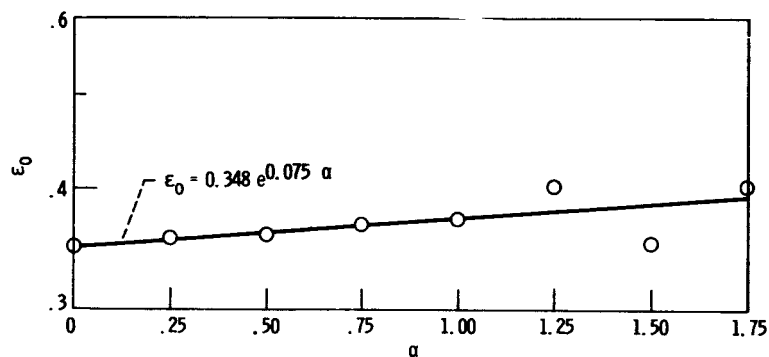Figure 8. – Raw data from X-Y recorder α = 1.75.
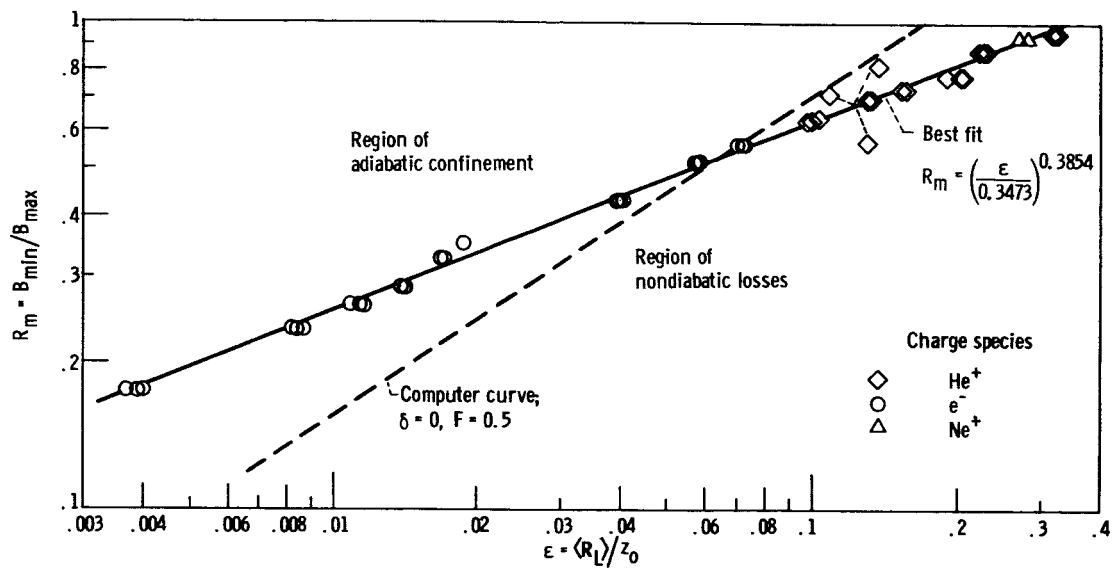
Figure 9. – Experimental data for particle motion near apparatus axis.
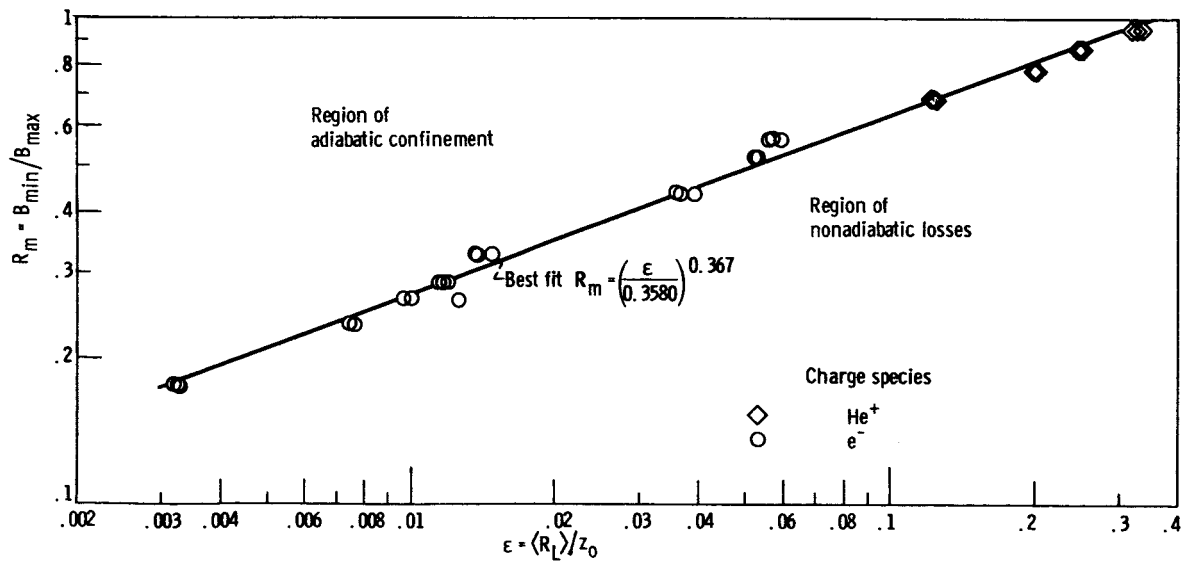
Figure 10. – Experimental data for $\alpha = 0.50$.

Figure 11. - Parameter A from experimental curves as function of α.

$A = 0.388 \, e^{-0.167 \, \alpha}$

Figure 12. - Parameter ε_0 from experimental curves as function of α.

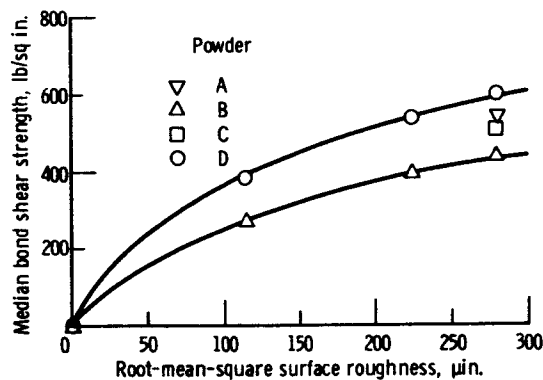$\varepsilon_0 = 0.348 \, e^{0.075 \, \alpha}$

Figure 3. – Median bond shear strength (50 percent
failed value) for four alumina spray powders on
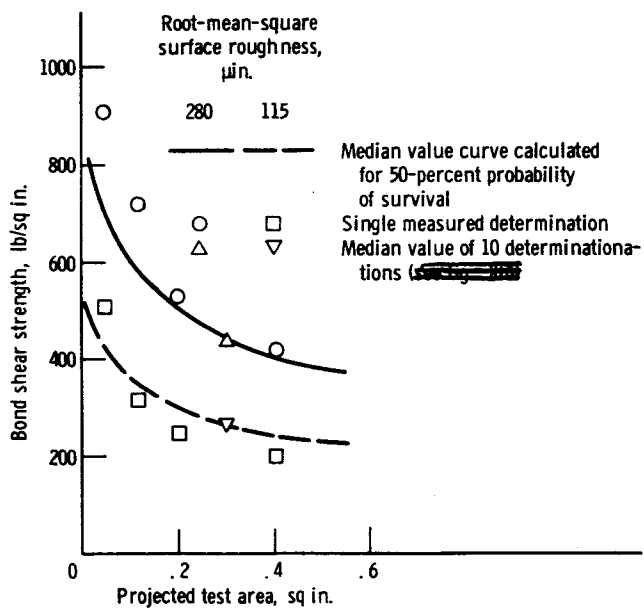stainless steel substrates of varying roughness.

Figure 4. – Effect of projected test area on measured and calcu-
lated bond shear strength of powder-B coatings at two surface
roughnesses.